Low-loss curved subwavelength grating waveguide based on index engineering

Zheng Wang*[a, b, †], Xiaochuan Xu*[c,†], D.L. Fan[a,d], Yaguo Wang[a, d] and Ray T. Chen*[a,b,c]
[a]Materials Science and Engineering Program, Texas Materials Institute, The University of Texas at Austin, Austin, TX USA 78712;
[b]Dept. of Electrical and Computer Engineering, The University of Texas at Austin, 10100 Burnet Rd., MER 160, Austin, TX USA 78758;
[c]Omega Optics, Inc., 8500 Shoal Creek Blvd., Bldg. 4, Suite 200, Austin, TX USA 78757;
[d]Dept. of Mechanical Engineering, University of Texas at Austin, Austin, TX USA 78712;
[†]These authors equally contributed to this work.

ABSTRACT

Subwavelength grating (SWG) waveguide is an intriguing alternative to conventional optical waveguides due to its freedom to tune a few important waveguide properties such as dispersion and refractive index. Devices based on SWG waveguide have demonstrated impressive performances compared to those of conventional waveguides. However, the large loss of SWG waveguide bends jeopardizes their applications in integrated photonics circuits. In this work, we propose that a pre-distorted refractive index distribution in SWG waveguide bends can effectively decrease the mode mismatch noise and radiation loss simultaneously, and thus significantly reduce the bend loss. Here, we achieved the pre-distortion refractive index distribution by using trapezoidal silicon pillars. This geometry tuning approach is numerically optimized and experimentally demonstrated. The average insertion loss of a 5 μm SWG waveguide bend can be reduced drastically from 5.58 dB to 1.37 dB per 90 ° bend for quasi-TE polarization. In the future, the proposed approach can be readily adopted to enhance performance of an array of SWG waveguide-based photonics devices.

Keywords: Subwavelength structures, Subwavelength grating waveguide, Subwavelength grating waveguide bend, Low-loss waveguide bend, Curved waveguide

1. INTRODUCTION

Silicon photonics has been attracting intensive interest in the last decade [1] due to its great potential in realizing low cost photonic chips with the readily-available CMOS manufacture technology [2]. However, the fact that silicon does not have either a direct band gap or the second-order nonlinearity makes it a great challenge to generate or control photons. Hybrid integration of silicon and functional cladding material has been considered as a potential solution to this issue [3]. Plenty structures, such as slot waveguides [4-6] and photonic crystal waveguides [7-9], have been exploited to enhance the light-matter interaction. Subwavelength grating (SWG) waveguide, comprised of periodically arranged high refractive index and low refractive index materials with a pitch less than one wavelength, has received considerable attention in recent years [10-21]. Bloch modes can be supported by this periodic arrangement of high refractive index and low refractive index materials, and therefore theoretically photons can propagate without being attenuated by the discontinuity of mediums [10, 11]. SWG provides another dimension of freedom to precisely control a few important waveguide properties such as refractive index [12-14], dispersion[15], and mode overlap volume [16], which are determined by materials constituting the waveguides as demonstrated previously. The control of these properties enables significant improvements over conventional waveguide based devices such as grating couplers [12, 15], directional couplers [17] , sensors [18], filters [19] and modulators [20]. One critical problem remaining unresolved is the large loss of SWG waveguide bends. For instance, a 10 μm radius 90 ° bend has an insertion loss of ~1.5dB [21]. To avoid the substantial loss introduced by SWG waveguide bends, SWG waveguide is tapered to conventional strip waveguides before reaching a bend and further tapered back to SWG waveguides afterwards [11]. Although the strip waveguide bends can significantly reduce the loss, the taper adds additional loss and wastes the precious silicon chip surface [21].

* wangzheng@utexas.edu; xiaochuan.xu@omegaoptics.com; chenrt@austin.utexas.edu

Optical Interconnects XVI, edited by Henning Schröder, Ray T. Chen, Proc. of SPIE Vol. 9753, 975318

Therefore, to achieve the goal of building integrated photonics system with entirely SWG waveguides, a low loss and small bend radius SWG bend is highly desirable. In this paper, we propose and experimentally demonstrate that the loss of SWG bends can be significantly reduced by optimizing the refractive index distribution via geometrical tuning of silicon pillars.

2. THEORETICAL ANALYSIS OF THE BEND LOSS

Fig. 1(a) shows a 3D schematic of a typical SWG waveguide, where Λ is the period of the SWG structure, l, w, and h are the length, width, and height of silicon pillars, respectively. In our simulation and experiments, SU-8 (n=1.575) is selected as the cladding material. The period Λ is 300 nm. A typical silicon pillar has a geometry of $l \times w \times h$= 150 nm × 500 nm × 250 nm without further optimization [11]. To simplify the analysis, two approximations are adopted sequentially without losing generality. Firstly, SWG waveguide is approximated as a uniform strip waveguide of an equivalent refractive index n=2.70, which corresponding to a ratio of silicon to SU-8 of 0.5 by using the first order effective medium theory (EMT) [12]. Then the 3D strip waveguide is further simplified into 2D waveguide through effective index approximation, as shown in Fig. 1(b) [22]. In a cylindrical coordinate system, the refractive index distribution of a bend shown in Fig. 1(b) can be given by

$$n_{eq}(\rho) = \begin{cases} n_{cl} & \rho < r_1, \rho > r_2 \\ n_{co} & r_1 \le \rho \le r_2 \end{cases} \tag{1}$$

n_{cl} and n_{co} are the effective refractive index of the cladding (n_{cl} =1.575) and core of a waveguide (n_{co} = 2.2), respectively. r_1 and r_2 denote the radius of the inner and outer edge, respectively. To unveil the source of bend loss, conformal transformation method, which has been widely used to analyze conventional strip waveguide bends [22-26], is applied. By using the conformal transformation $W = r_2 \ln Z / r_2$, a bend in Z plane can be taken equivalently as a straight waveguide in W plane, as shown in Fig. 1(b) and Fig. 1(c) [23].

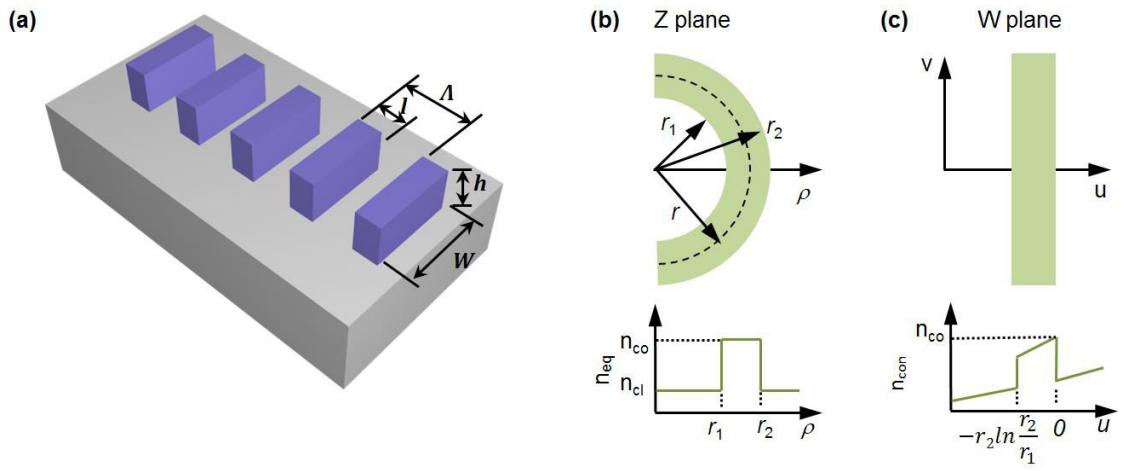

Fig. 1. (a) 3D schematic of an SWG waveguide bend. Refractive index distribution in (b) Z plane and (c) W plane.

Here, $Z = x + yi$ and $W = u + vi$. Fig. 1(c) shows the geometry and equivalent index distribution in W space with transformed Cartesian coordinate system. The first order approximation of transformed equivalent index $n_{con}(u)$ can be calculated by

$$n_{con}(u) = n_{eq}(r_2 e^{u/r_2}) e^{u/r_2} \tag{2}$$

Fig. 2(a) shows the $n_{con}(u)$ with different bend radius r. The red curve represents the conformal transformation of a straight waveguide in W plane. With the decrease of bend radius, the refractive index distribution in W plane becomes asymmetric and tilted, which shifts the mode to the outer edge of a SWG waveguide bend as shown by the colored curves in Fig. 2(b). The delocalization of optical modes due to bending leads to a mode mismatch between straight and curved waveguide segments and an increase of radiation loss.

To quantify the change of refractive index distribution induced by a bend, we define a distortion factor D as

$$D = 1 - \frac{\left|\int n_{con}(u) n_{con}^{r=\infty}(u) du\right|^2}{\int |n_{con}(u)|^2 du \int \left|n_{con}^{r=\infty}(u)\right|^2 du} \tag{3}$$

Here, $n_{con}^{r=\infty}(u)$ is the refractive index distribution in W plane after conformal transformation when the bend radius is infinite, as shown by the black curve in Fig. 2(a).

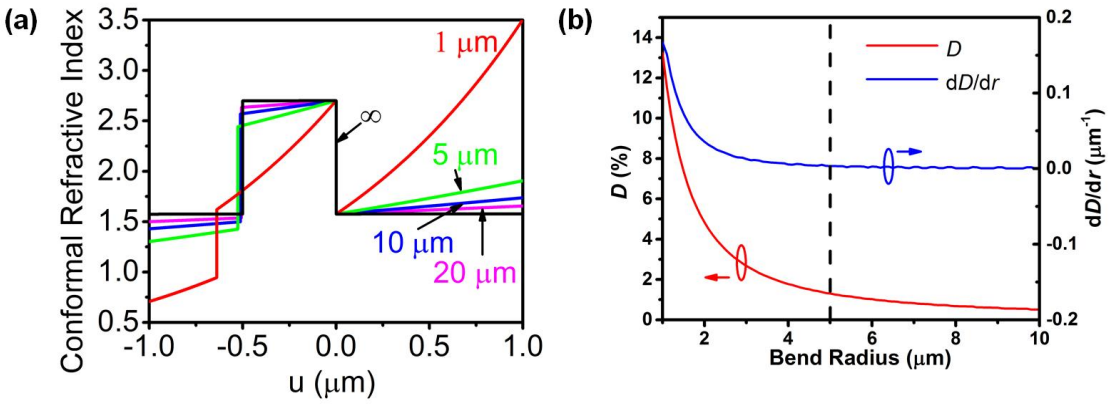

Fig. 2. (a) The refractive index distribution of bends of different radii in W plane. (b) The refractive index distortion D (red) and distortion changing rate dD/dr (blue) as a function of bend radius.

As shown by the red curve in Fig. 2(b), refractive index distortion D increases with the decrease of the bend radius. The blue curve in Fig. 2(b) is the D changing rate as a function of the bend radius r (dD/dr). When the bend radius r > 5 μm, D is less than 1% and insensitive to the bend radius. Thus, we choose to study the case of r= 5 μm.

3. PRE-DISTORTION COMPENSATION METHOD

To eliminate the distortion, ideally the refractive index distribution of a bend in Z plane must satisfy the condition of $n_{con}(u) = n_{con}^{r=\infty}(u)$, which is extremely difficult to achieve due to the limited control of the distribution of refractive index of conventional waveguides. SWG waveguides, however, provide the freedom for tailoring the refractive index and makes it attainable to minimize D. According to Eq. (2), $n_{eq}(r_2 e^{u/r_2})$ should be equivalent to $n_{con} e^{-u/r_2}$ to cancel the u dependent term. Thus, ideally the refractive index distribution in Z plane should follow the equation as below:

$$n_{eq}(\rho) = \begin{cases} n_{cl} r_2/\rho & \rho < r_1 or \rho > r_2 \\ n_{co} r_2/\rho & r_1 \le \rho \le r_2 \end{cases}. \tag{4}$$

One can notice that the refractive index of the cladding is not tunable once decided. However, since the majority of mode is concentrated in the high index region, the distortion of the cladding refractive index can be safely ignored. According

to Eq. (4), $n_{eq}(r_2) = n_{co}$ and $n_{eq}(r_1) = n_{co}\, r_2 / r_1$. Therefore, $n_{eq}(r_2)$ and $n_{eq}(r_1)$ equal to 2.98 and 2.70, respectively. Considering it is not realistic to fabricate a SWG waveguide with the refractive index distribution described by Eq. (4), and knowing $r >> w$, we took a linear approximation and simplify the equation to

$$n'_{eq}(\rho) = \frac{n_{eq}(r_2) - n_{eq}(r_1)}{r_2 - r_1}(\rho - r_2) + n_{eq}(r_2) \quad . \qquad (5)$$
$$r_1 \le \rho \le r_2$$

Fig. 3(a) illustrates this linear pre-distortion compensation method. The left one represents a pre-distortion index distribution and the right one is the corresponding refractive index distribution in Z plane. To validate this approximation, we keep the refractive index of the outer edge at 2.70 and scan the refractive index of the inner edge, as shown in Fig. 3(b). When the refractive index of the inner edge equals 2.98, *D* is minimized. The value is very close to that calculated from Eq. (4). The insets of Fig. 3(b) show the fundamental quasi-TE mode profiles of three representative waveguides: a curved SWG waveguide with the original symmetric equivalent index distribution (top left), a curved SWG waveguide with the optimized asymmetric equivalent index distribution(center), and a straight SWG waveguide with the original symmetric equivalent index distribution (top right). The mode profiles of waveguide bends are simulated via the 3D finite-difference time domain (FDTD) method (Rsoft v8.1) at 1550 nm. It can be found that the pre-distortion compensation significantly reduces the mode delocalization.

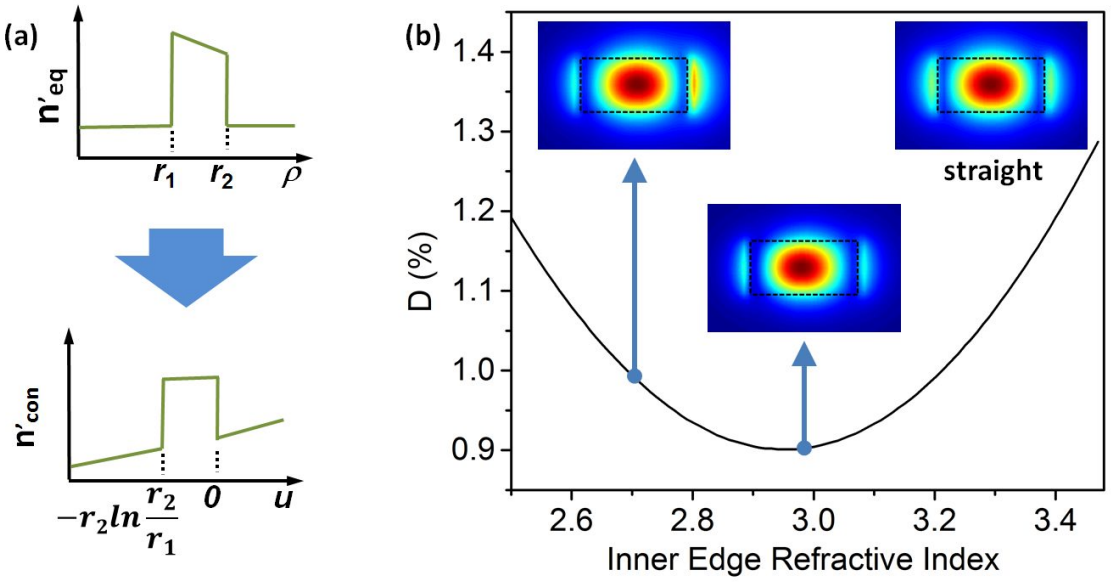

Fig. 3. (a) The pre-distortion compensation method. (b)Refractive index distortion versus inner edge refractive index with a fixed outer edge refractive index of 2.70. Insets: the mode profiles of bends with different equivalent refractive index distribution. The mode profile of the straight waveguide is provided at the top right as a reference.

To implement the proposed approach into SWG waveguide bends, trapezoidal silicon pillars are exploited to create the asymmetric equivalent index distribution. A schematic of trapezoidal silicon pillars is shown in Fig. 4(a). The top and bottom base can be optimized to minimize the bend loss. According to Eq. (5), the refractive index of the inner side needs to be increased to compensate the refractive index distortion due to the bending and to shift the mode back to the center. To verify the aforementioned theoretical analysis, we used full 3D FDTD simulation to scan parameters of the top and bottom bases of the trapezoidal silicon pillars. The simulation results are summarized in a contour plot as shown in Fig. 4(b). It is found that a trapezoidal silicon pillar with 140 nm top base and 210 nm bottom base offers the minimized bend loss of 0.192 dB per 90 °bend, which is 50.1% of the bend loss (0.383 dB per 90 °bend) of a conventional rectangular silicon pillar. The calculated effective indices of the optimized geometry of silicon pillars

at the outer (2.60) and inner edges (3.16) are very close to analytical results of 2.70 and 2.98, respectively. The discrepancies are can be attributed primarily to the approximations of EMT and effective index.

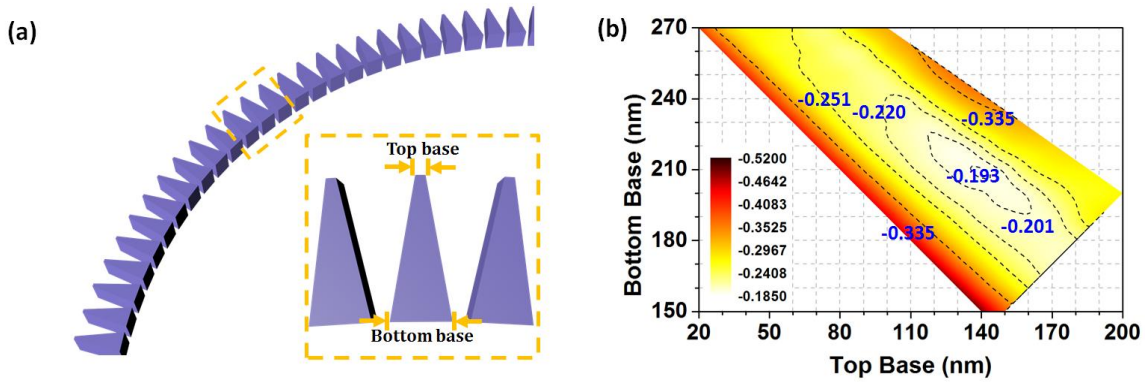

Fig. 4. (a) Schematic of trapezoidal silicon pillars. (b) Contour plot of bend loss for different top and bottom bases.

4. EXPERIMENTAL DEMONSTRATION

Non-tuned rectangle (150 nm top base and 150 nm bottom base) and optimally-tuned trapezoid (140 nm top base and 210 nm bottom base) have been fabricated for demonstration. The devices are made on a SOI wafer consisting of a 250 nm thick top silicon layer (n=3.476) lying on a 3 μm thick buried oxide (BOX, n=1.45) layer (manufactured by Soitec). All structures are patterned in a single E-beam lithography (JEOL 6000 FSE) step. The patterns are then transferred into the underneath silicon layer through reactive-ion-etching (PlasmaTherm 790). The agreement of the morphology of the devices with the design is confirmed by scanning electron microscopy (ZEISS Neon 40) as shown in Fig. 5(a). Each device has four 90 °bends. Fig. 5(b) and (c) show the high magnification SEM images of the two types of SWG waveguide bends: non-tuned and optimally tuned.

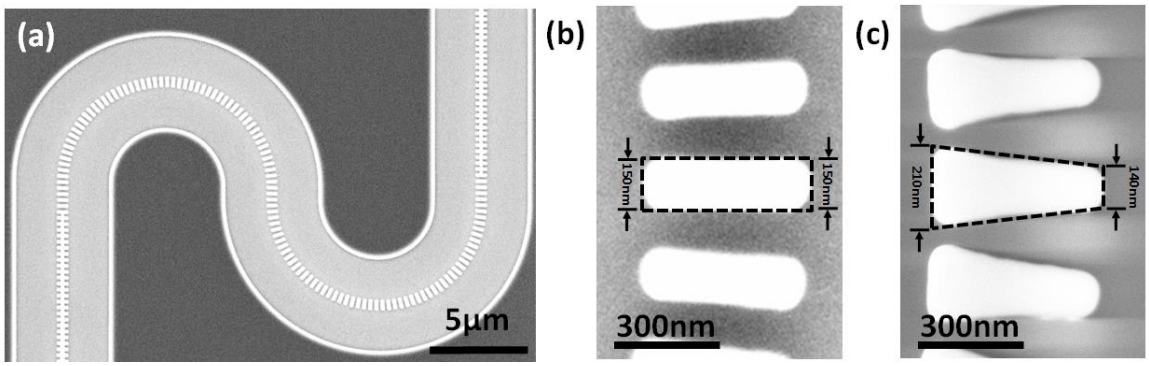

Fig. 5. (a) SEM image of a typical device. SEM images of (b) non-tuned silicon pillars, and (c) optimally tuned silicon pillars.

After spin-coating the SU-8 cladding, the devices are tested in a customized grating coupler alignment system, employed in our previous work [12, 14, 27]. In our experiment, the two types of SWG bends have been fabricated and tested three times. Spectra of all devices without subtracting the grating couplers' response from 1530 nm to 1580 nm is shown in Fig. 6(a). The insertion loss of the two types of bends is shown in Fig. 6(b). For 1550nm, one could find the loss of SWG bends built with optimized trapezoidal silicon pillars is as low as 1.10dB per 90 °bend, only 20.3% of that of the non-tuned cases (5.43dB per 90 °bend). Compared to the earlier demonstration of 10 μm SWG bend [21], we are able to reduce the bend radius to 5 μm without increasing the insertion loss. When the pillars are over-tuned, the refractive index distortion and mode mismatch increase, and thus the loss increases. Although the insertion loss of the bends are higher

than that of the theoretical prediction, which could be attributed to the surface roughness of the silicon pillars, the experimental results clearly demonstrate that the loss of SWG bends can be significantly reduced by optimizing the shapes of the silicon pillars.

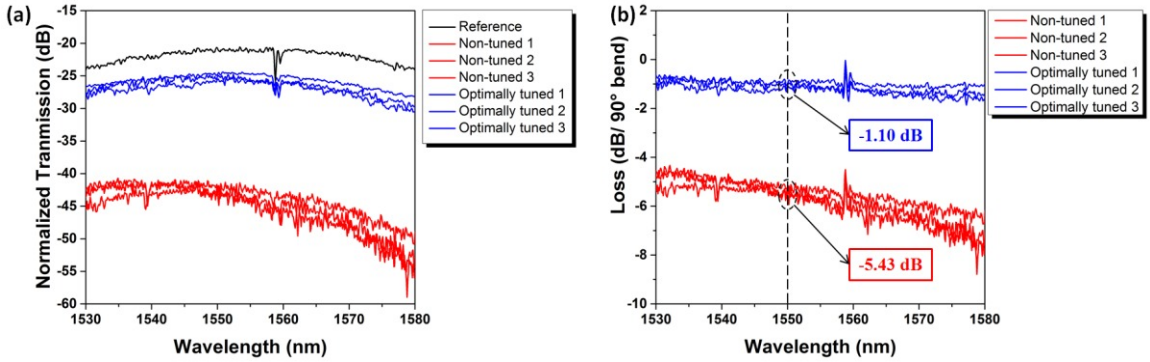

Fig. 6. (a)Transmission spectra of the two types of SWG bends. (b) Insertion loss of the two types of SWG bends.

5. CONCLUSION

In conclusion, via theoretical analysis, numerical simulation, and experimental study, we demonstrate that through pre-distortion compensation with optimized trapezoidal silicon pillars, the insertion loss of SWG waveguide bends can be substantially reduced. Comparing to conventional SWG waveguide bends which use rectangular silicon pillars, an average reduction of 79.7% of the insertion loss has been achieved experimentally via the optimized trapezoidal silicon pillars. This study paves a road towards achieving all SWG waveguide based optical devices and circuits.

REFERENCES

[1] R. Soref, "The past, present, and future of silicon photonics," IEEE J. Sel. Topics Quantum Electron., 12(6), 1678-1687 (2006).

[2] M. Hochberg, N. C. Harris, R. Ding *et al.*, "Silicon photonics: the next fabless semiconductor industry," IEEE Solid State Circuits Mag., 5(1), 48-58 (2013).

[3] M. J. R. Heck, J. F. Bauters, M. L. Davenport *et al.*, "Hybrid Silicon Photonic Integrated Circuit Technology," IEEE J. Sel. Topics Quantum Electron., 19(4), 6100117 (2013).

[4] C. A. Barrios, K. B. Gylfason, B. Sanchez *et al.*, "Slot-waveguide biochemical sensor," Opt. Lett., 32(21), 3080-3082 (2007).

[5] C. Koos, P. Vorreau, T. Vallaitis *et al.*, "All-optical high-speed signal processing with silicon-organic hybrid slot waveguidesx," Nat. Photonics, 3(4), 216-219 (2009).

[6] A. H. J. Yang, S. D. Moore, B. S. Schmidt *et al.*, "Optical manipulation of nanoparticles and biomolecules in sub-wavelength slot waveguides," Nature, 457(7225), 71-75 (2009).

[7] J. M. Brosi, C. Koos, L. C. Andreani *et al.*, "High-speed low-voltage electro-optic modulator with a polymer-infiltrated silicon photonic crystal waveguide," Opt. Express, 16(6), 4177-4191 (2008).

[8] C. Y. Lin, X. L. Wang, S. Chakravarty *et al.*, "Electro-optic polymer infiltrated silicon photonic crystal slot waveguide modulator with 23 dB slow light enhancement," Appl. Phys. Lett., 97(9), 093304 (2010).

[9] X. L. Wang, C. Y. Lin, S. Chakravarty *et al.*, "Effective in-device r(33) of 735 pm/V on electro-optic polymer infiltrated silicon photonic crystal slot waveguides," Opt. Lett., 36(6), 882-884 (2011).

[10] D. Ortega, J. M. Aldariz, J. M. Arnold *et al.*, "Analysis of "quasi-modes" in periodic segmented waveguides," J. Lightwave Technol., 17(2), 369-375 (1999).

[11] P. J. Bock, P. Cheben, J. H. Schmid *et al.*, "Subwavelength grating periodic structures in silicon-on-insulator: a new type of microphotonic waveguide," Opt. Express, 18(19), 20251-20262 (2010).

[12]X. C. Xu, H. Subbaraman, J. Covey *et al.*, "Complementary metal-oxide-semiconductor compatible high efficiency subwavelength grating couplers for silicon integrated photonics," Appl. Phys. Lett., 101(3), 031109 (2012).
[13]Y. Zhang, A. Hosseini, X. C. Xu *et al.*, "Ultralow-loss silicon waveguide crossing using Bloch modes in index-engineered cascaded multimode-interference couplers," Opt. Lett., 38(18), 3608-3611 (2013).
[14]Z. Wang, H. Yan, S. Chakravarty *et al.*, "Microfluidic channels with ultralow-loss waveguide crossings for various chip-integrated photonic sensors," Opt. Lett., 40(7), 1563-1566 (2015).
[15]X. C. Xu, H. Subbaraman, J. Covey *et al.*, "Colorless grating couplers realized by interleaving dispersion engineered subwavelength structures," Opt. Lett., 38(18), 3588-3591 (2013).
[16]J. G. Wangueemert-Perez, P. Cheben, A. Ortega-Monux *et al.*, "Evanescent field waveguide sensing with subwavelength grating structures in silicon-on-insulator," Opt. Lett., 39(15), 4442-4445 (2014).
[17]R. Halir, A. Maese-Novo, A. Ortega-Monux *et al.*, "Colorless directional coupler with dispersion engineered sub-wavelength structure," Opt. Express, 20(12), 13470-13477 (2012).
[18]V. Donzella, A. Sherwali, J. Flueckiger *et al.*, "Design and fabrication of SOI micro-ring resonators based on sub-wavelength grating waveguides," Opt. Express, 23(4), 4791-4803 (2015).
[19]J. J. Wang, I. Glesk, and L. R. Chen, "Subwavelength grating filtering devices," Opt. Express, 22(13), 15335-15345 (2014).
[20]S. Inoue, and A. Otomo, "Electro-optic polymer/silicon hybrid slow light modulator based on one-dimensional photonic crystal waveguides," Appl. Phys. Lett., 103(17), 171101 (2013).
[21]V. Donzella, A. Sherwali, J. Flueekiger *et al.*, "Sub-wavelength grating components for integrated optics applications on SOI chips," Opt. Express, 22(17), 21037-21050 (2014).
[22]F. Ladouceur, and P. Labeye, "A new general approach to optical waveguide path design," J. Lightwave Technol., 13(3), 481-492 (1995).
[23]M. Heiblum, and J. H. Harris, "Analysis of Curved Optical-Waveguides by Conformal Transformation," IEEE J. Quantum Electron., 11(2), 75-83 (1975).
[24]M. K. Smit, E. C. M. Pennings, and H. Blok, "A Normalized Approach to the Design of Low-Loss Optical Wave-Guide Bends," J. Lightwave Technol., 11(11), 1737-1742 (1993).
[25]W. Berglund, and A. Gopinath, "WKB analysis of bend losses in optical waveguides," J. Lightwave Technol., 18(8), 1161-1166 (2000).
[26]D. P. Cai, J. H. Lu, C. C. Chen *et al.*, "High Q-factor microring resonator wrapped by the curved waveguide," Sci. Rep., 5, 10078 (2015).
[27]X. C. Xu, H. Subbaraman, S. Chakravarty *et al.*, "Flexible Single-Crystal Silicon Nanomembrane Photonic Crystal Cavity," ACS Nano, 8(12), 12265-12271 (2014).